

Unraveling the dynamical origin of intense fifth harmonic generation from H_2^+ in a linearly laser field

Ling-Ling Du(杜玲玲), Jiang-Yue Bu(卜江越), Cun-Bin Chen(陈存斌), and Xiao-Xin Zhou(周效信)
Citation: Chin. Phys. B, 2025, 34 (**12**): 123301. DOI: 10.1088/1674-1056/ae23ab
http://cpb.iphy.ac.cn; http://iopscience.iop.org/cpb

What follows is a list of articles you may be interested in

Theoretical investigation of elliptical high-order harmonic generation from H_2^+ in two-color cross-linearly-polarized laser fields

Cai-Ping Zhang(张彩萍), Si-Hui Wang(王思慧), Yu-Zhi Chen(陈育之), Xin-Ru Du(杜欣茹), and Xiang-Yang Miao(苗向阳)
Chin. Phys. B, 2025, 34 (**8**): 083301. DOI: 10.1088/1674-1056/add00a

Experimental manipulation of fine structures in high harmonic spectrum of aligned CO_2 molecules

Ge-Wen Wang(王革文), Yi-Wen Zhao(赵逸文), Yi-Chen Wang(王一琛), Jing Ma(马婧), Bo-Dun Liu(刘博敦), Wei Jiang(姜威), Hong-Jing Liang(梁红静), and Ri Ma(马日)
Chin. Phys. B, 2025, 34 (**6**): 063301. DOI: 10.1088/1674-1056/adab65

Channel competition in dissociation of ammonia clusters ($n \leq 5$) induced by femtosecond laser fields

Tao Yang(杨涛), Xinyu Zhang(张馨予), Xing Li(李兴), Wankai Li(李万凯), Menghao Wei(卫孟昊), Dongdong Zhang(张栋栋), Lanhai He(赫兰海), and Dajun Ding(丁大军)
Chin. Phys. B, 2025, 34 (**3**): 033302. DOI: 10.1088/1674-1056/ada552

Time-energy distribution of photoelectron from atomic states with different magnetic quantum numbers in elliptically polarized laser fields

Jingyang Xu(徐菁阳), Li Guo(郭丽), Xin Qi(齐昕), Ronghua Lu(陆荣华), Min Zhang(张敏), Jingtao Zhang(张敬涛), and Jing Chen(陈京)
Chin. Phys. B, 2024, 33 (**9**): 093301. DOI: 10.1088/1674-1056/ad58b3

Excitation and ionization of OCS molecules in strong UV and NIR laser fields

Huijun Shi(师慧军), Yang Liu(刘洋), Tian Sun(孙添), Hang Lv(吕航), and Haifeng Xu(徐海峰)
Chin. Phys. B, 2024, 33 (**7**): 073301. DOI: 10.1088/1674-1056/ad3035

SPECIAL TOPIC — Ultrafast physics in atomic, molecular and optical systems

Unraveling the dynamical origin of intense fifth harmonic generation from H_2^+ in a linearly laser field

Ling-Ling Du(杜玲玲)[1,†], Jiang-Yue Bu(卜江越)[1], Cun-Bin Chen(陈存斌)[1], and Xiao-Xin Zhou(周效信)[2,3,‡]

[1] *School of Physics, Ningxia University, Yinchuan* 750021, *China*
[2] *College of Physics and Electronic Engineering, Northwest Normal University, Lanzhou* 730070, *China*
[3] *Shenzhen Key Laboratory of Ultra-Intense Laser and Advanced Material Technology, College of Engineering Physics, Shenzhen Technology University, Shenzhen* 518118, *China*

(Received 9 September 2025; revised manuscript received 12 November 2025; accepted manuscript online 25 November 2025)

A systematic investigation of the fifth-harmonic generation in H_2^+, driven in the vicinity of a five-photon resonance by a linearly polarized laser field, has been carried out by numerically solving the full three-dimensional time-dependent Schrödinger equation. We observe a pronounced enhancement of the fifth harmonic, while the intensities of the adjacent harmonics are significantly suppressed. Our analysis shows that such an enhancement of the fifth harmonic is mainly caused by the multiphoton resonance transition, as well as multichannel interference. In addition, we investigate the dependence of harmonic emission on laser intensity and molecular orientation to identify the optimal conditions for enhancing the fifth-harmonic generation. Our results provide useful insights for producing coherent ultraviolet radiation at 106 nm experimentally.

Keywords: intense fifth-harmonic generation, hydrogen molecule ions, multiphoton resonance, multichannel interference

PACS: 33.80.Rv, 42.50.Hz, 42.65.–k

DOI: 10.1088/1674-1056/ae23ab **CSTR:** 32038.14.CPB.ae23ab

1. Introduction

High-order harmonic generation (HHG) serves not only as an excellent source of coherent femtosecond (fs) pulses from the extreme ultraviolet (XUV) to the soft x-ray region[1–4] but also as a powerful tool for probing ultrafast electron dynamics and material structural properties.[5–10] The underlying physical mechanism of HHG in gases is well described by the three-step model.[11] First, an electron tunnels through the potential barrier formed by the combined laser and Coulomb field. Second, the freed electron is accelerated by the laser field. Finally, upon reversal of the laser field direction, the electron may be driven back toward the parent ion and undergo recombination, resulting in the emission of a high-energy photon. In this picture, HHG spectra typically display a broad structure consisting of a plateau region that extends over many harmonic orders, thereby producing coherent radiation across a wide range of the XUV spectrum, but with inherently low photon conversion efficiency.[12] However, coherent quasi-monochromatic extreme ultraviolet (QM-XUV) pulses are of great significance for applications in many advanced experiments, such as XUV pump–probe spectroscopy for tracking fs-scale electronic dynamics,[13] XUV diffractive imaging achieving high spatial resolution,[14] time-resolved photoemission techniques for both band structure mapping and surface topology analysis,[15,16] and XUV nonlinear optics research to generate highly charged ions in noble gases.[17]

In order to obtain intense fs QM-XUV pulses, a traditional approach involves isolating individual harmonics from the broadband harmonic spectrum using XUV optics.[18] However, this wavelength-selection technique introduces significant harmonic flux attenuation. This is a critical challenge for HHG-based sources intended for experiments requiring intense fs QM-XUV radiation. To overcome this obstacle, there are two main approaches to enhance harmonic conversion efficiencies: the first is a waveform-synthesized laser field by using a multi-color field,[19,20] and the second is resonant transition between autoionizing states and the ground state,[21] which can selectively enhance a single high-order harmonic while greatly suppressing adjacent harmonics. For below-threshold harmonics, the intensity of a single harmonic can be enhanced by employing methods of nonlinear optics[22] and utilizing resonant transition from excited states to the ground state.[23–27] Experimentally, using a short-wavelength laser in the multiphoton ionization regime, Singh *et al.* achieved a significant enhancement in seventh harmonic generation from Ga^+ ions, demonstrating a resonant intensity enhancement ratio of 714 relative to the adjacent fifth and ninth harmonics.[23]

†Corresponding author. E-mail: lingling_du@nxu.edu.cn
‡Corresponding author. E-mail: zhouxx@nwnu.edu.cn

© 2025 Chinese Physical Society and IOP Publishing Ltd. All rights, including for text and data mining, AI training, and similar technologies, are reserved.

Theoretically, Camp *et al.* reported enhancements of the 7th, 9th, and 11th harmonics, and these enhancements arise from multiphoton resonances between the ground state and Stark-shifted excited states in He.[27] Research on absorption-limited conversion efficiency has shown that the HHG conversion efficiency is proportional to $|A_q/\sigma_q|^2$,[28] where A_q and σ_q are the amplitude of the oscillating dipole and the absorption cross section at the harmonic frequency ω_q, respectively. Thus, the HHG conversion efficiency can be increased in two ways: by increasing A_q, or by reducing σ_q of HH photons. By choosing the molecules and noble gas clusters as generating media, the excitation of resonances can increase the single-atom response A_q.

In this paper, we explore the generation of a high-efficiency harmonic of H_2^+ in an intense laser field by solving the full three-dimensional time-dependent Schrödinger equation (TDSE). We find that using the frequency-doubled light of a Nd:YAG laser (which emits light at 1064 nm) produces a pronounced enhancement of the fifth harmonic, while the intensities of the adjacent harmonics are completely suppressed. We reveal the mechanism by varying the laser's wavelength. In order to determine optimal conditions for enhanced fifth harmonic, we further investigate the variation of fifth-harmonic radiation with the laser's intensity and orientation angle. Recently, Bengtsson *et al.* explored the control of free induction decay — a process analogous to atomic resonance. They found that absorption by the medium can be notably suppressed by adjusting the propagation direction of the spontaneously emitted light.[26] Their experimental results also indicate that this light emitted via free induction decay to the ground state exhibits coherence properties similar to those of HHG. Thus, our results offer valuable guidance for producing coherent ultraviolet radiation at 106 nm in experiments.

2. Theoretical methods

The molecular axis of H_2^+ is aligned along the z-axis, with nuclei fixed at $-a$ and a ($R = 2a$). HHG can be studied by solving the TDSE[29–31] in prolate spheroidal coordinates (ξ, η, φ). In atomic units, the full three-dimensional TDSE is given by

$$\mathrm{i}\frac{\partial\Psi(\xi,\eta,\varphi,t)}{\partial t} = \left[H_0(\xi,\eta)+V(\xi,\eta,\varphi,t)\right]\Psi(\xi,\eta,\varphi,t), \quad (1)$$

where $V(\xi,\eta,\varphi,t)$ is the interaction potential, it is written as

$$\begin{aligned} &V(\xi,\eta,\varphi,t)\\ &= aE(t)\left[\xi\eta\cos\theta+\sqrt{(\xi^2-1)(1-\eta^2)}\cos\varphi\sin\theta\right], \end{aligned} \quad (2)$$

where θ is the orientation angle between the polarization vector of the laser field and the molecular axis. $E(t) = E_0\sin^2(\pi t/T)\sin(\omega t)$ is the laser field. $H_0(\xi,\eta)$ represents the field-free Hamiltonian, which can be written as

$$\begin{aligned} H_0(\xi,\eta) = &-\frac{1}{2a^2(\xi^2-\eta^2)}\left[\frac{\partial}{\partial\xi}(\xi^2-1)\frac{\partial}{\partial\xi}\right.\\ &\left.+\frac{\partial}{\partial\eta}(1-\eta^2)\frac{\partial}{\partial\eta}+\frac{\xi^2-\eta^2}{(\xi^2-1)(1-\eta^2)}\frac{\partial^2}{\partial\varphi^2}\right]\\ &-\frac{2\xi}{a(\xi^2-\eta^2)}. \end{aligned} \quad (3)$$

Equation (1) is solved accurately and efficiently using the second-order split-operator method, expressed as

$$\begin{aligned} \Psi(t+\Delta t) \simeq &\exp\left(-\mathrm{i}H_0\frac{\Delta t}{2}\right)\exp\left[-\mathrm{i}V\left(t+\frac{\Delta t}{2}\right)\Delta t\right]\\ &\times\exp\left(-\mathrm{i}H_0\frac{\Delta t}{2}\right)\Psi(t)+O((\Delta t)^3). \end{aligned} \quad (4)$$

Then, the time-dependent population of every bound states and spectra of the produced HHG radiation can be obtained. The time-dependent population P_n of a particular quantum state $\varphi_n(\xi,\eta,\varphi)$ is evaluated from the following equation:

$$P_n(t) = \left|\langle\varphi_n(\xi,\eta,\varphi)|\Psi(\xi,\eta,\varphi,t)\rangle\right|^2. \quad (5)$$

The spectra density of the HHG radiation can be calculated by

$$S(\omega) = \frac{2\omega^4}{3\pi c^3}|\boldsymbol{d}(\omega)|^2, \quad (6)$$

where $\boldsymbol{d}(\omega)$ is the Fourier transform of $\boldsymbol{d}(t)$, and the time-dependent dipole moment is given by

$$\boldsymbol{d}(t) = \langle\Psi(t)|\boldsymbol{r}|\Psi(t)\rangle. \quad (7)$$

In our calculations, an absorbing layer is implemented between $R_b = 40$ and $R_{max} = 80$ a.u. to smoothly attenuate the wave function and prevent spurious reflections of the wave packet from the boundary. This ensures that outgoing electron currents are not reflected back into the simulation domain. For the time propagation, we use 4096 time steps per optical cycle, corresponding to a total of 81920 steps over the entire pulse duration of 20 optical cycles. This numerical scheme and parameter selection ensure the accuracy of the computed results.

3. Results and discussion

Figure 1 shows the calculated harmonic spectra of H_2^+ for the internuclear distances $R = 2$ a.u. (the equilibrium internuclear distance). To ensure the ionization process occurs in the same ionization regime, the Keldysh parameter γ is fixed. From the HHG spectrum with laser wavelength of 800 nm at a laser intensity of 1.5×10^{14} W/cm^2 shown in Fig. 1(a) (corresponding to a Keldysh parameter $\gamma = 1.3$), one can see that the harmonic spectrum satisfies the general characteristics: as the harmonic orders increase, the harmonic intensities decrease, and then a plateau region appears. A harmonic emission line,

which comes from the bound-bound resonant transition between the first excited state and the ground state, to the right of the harmonic of order 7 (H7) is clearly identified. However, as shown in Fig. 1(b), the harmonic spectrum produced by a 532 nm laser with an intensity of 3.5×10^{14} W/cm^2 (corresponding to a Keldysh parameter $\gamma = 1.3$) exhibits a significant enhancement in the plateau region. Specifically, the harmonic intensities in this region are approximately five orders of magnitude higher than those observed in Fig. 1(a). More significantly, there is a remarkably strong emission line at the fifth harmonic. Its intensity is not only comparable to that of the H1, but also three orders of magnitude higher than that of the H3 and H7. The intense harmonic H5 can easily produce coherent QM-XUV sources at 106 nm.

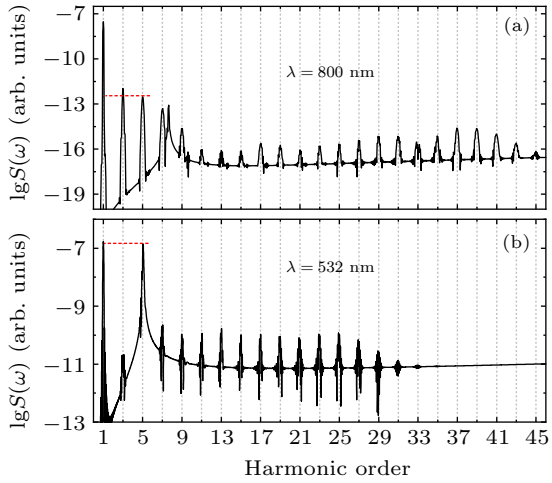


Fig. 1. Harmonic spectra of H_2^+ driven by laser fields at (a) an intensity of 1.5×10^{14} W/cm^2 and a wavelength of 800 nm, and (b) an intensity of 3.5×10^{14} W/cm^2 and a wavelength of 532 nm.

To explore the origin of the intense fifth harmonic, we show the harmonic spectra of H_2^+ at internuclear distances $R = 2$ a.u. with different wavelengths in Fig. 2(a). Both the pulse duration of 20 cycles and peak intensity of 3.5×10^{14} W/cm^2 are kept the same in all cases. As one can see, with the variation of the laser's wavelengths in a small range (from 515 nm to 545 nm), the peak intensities of the enhanced fifth harmonic depend sensitively on the laser's wavelength. From the comparison of the enlarged fifth harmonic shown in the inset, we can see that, with the change in the laser's wavelength from 515 nm to 545 nm, the H5 intensities first increase and then decrease. When the incident laser operates at 532 nm wavelength, the fifth harmonic exhibits maximum enhancement. However, when the laser's wavelength is tuned to the resonant wavelength (523 nm) of the fifth harmonic, the harmonic intensity is reduced compared to the off-resonance 532 nm excitation case. According to the previous studies,[31,32] with regard to the multi-photon process, the enhanced fifth harmonic of H_2^+ mainly comes from three kinds of contributions. In Fig. 3, we present the energy levels of the dressed states ($1\sigma_g$ and $1\sigma_u$) of H_2^+ and several instantaneous transitions between them. One is the transition from the dressed states of the same field-free excited state, which corresponds to transition 1. This process, predominant in the central part of the laser's pulse, is responsible for the usual odd harmonic generation. The other is a resonant transition between the different bound states, such as from the first excited $1\sigma_u$ state to the ground $1\sigma_g$ state of H_2^+, which corresponds to transition 2. This process can persist until the end of the laser field and may continue beyond it. The last is the interference effect between transition 1 and transition 2. In order to investigate which types of transitions contribute to the enhancement of the fifth harmonic, we show the populations of the $1\sigma_u$ state with different wavelengths in Fig. 2(b). The population can be obtained by projecting the time-dependent wave function onto the free-field $1\sigma_u$ state near the end of the falling edge of the laser pulse. The laser's parameters are the same as those in Fig. 2(a). To enable direct comparison, figure 2(c) presents both the H5 peak intensity from Fig. 2(a) and the final population from Fig. 2(b) as functions of the laser's wavelength. As the laser's wavelength increases from 515 nm to 545 nm, the final population of the $1\sigma_u$ state first increases and then decreases. The variation trend of the H5 peak intensity with laser wavelength is analogous to that of the final population. This phenomenon indicates that the contribution of transition 2 is important. Moreover, the population reaches its maximum at an off-resonance wavelength of 532 nm, exceeding that at the resonance wavelength of 523 nm. It indicates that more electrons are excited to the first excited $1\sigma_u$ state of H_2^+ via

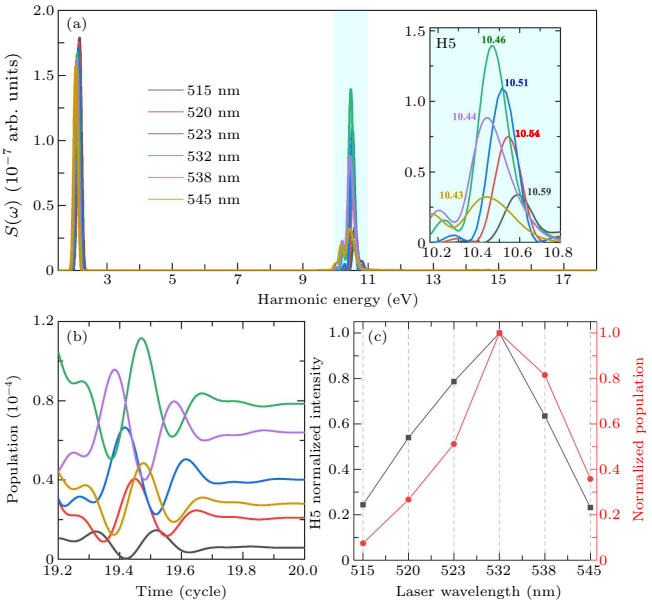


Fig. 2. (a) Harmonic spectra of H_2^+ driven by laser fields at an intensity of 3.5×10^{14} W/cm^2 with different wavelengths. (b) The corresponding population of the first excited state $1\sigma_u$ of H_2^+ near the end of the laser's pulse. (c) The H5 peak intensity and the final population of the $1\sigma_u$ state as a function of the laser's wavelength.

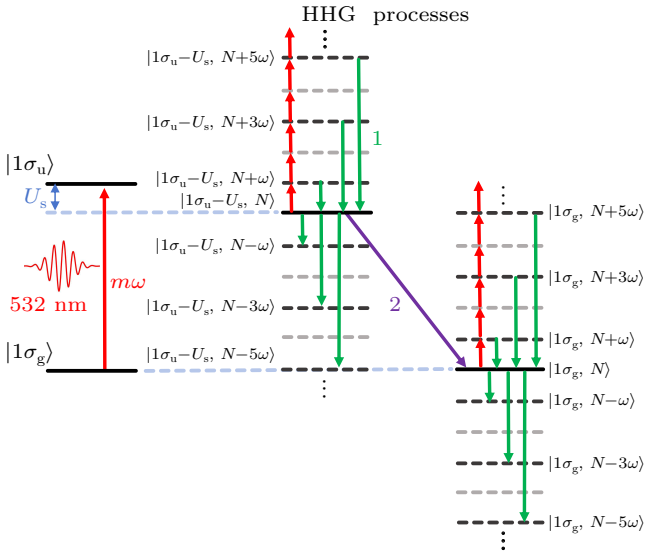


Fig. 3. The physical mechanisms of the intense fifth harmonic generation. The red arrows indicate the multiphoton absorption process, the green arrows indicate the transition between the dressed states, and the purple arrows indicate the resonant transition between the different bound states.

a five-photon resonance process at 532 nm, which can be attributed to the AC Stark shift of this state. Therefore, the influence of the AC Stark effect on the $1\sigma_u$ state must be taken into account. Furthermore, we observe that the population at 538 nm is larger than that at 523 nm, whereas the H5 peak intensity at 523 nm is greater than that at 538 nm. A similar discrepancy is also evident at wavelengths of 520 nm and 545 nm. These results imply that resonant transition is not the only reason for the enhancement of the fifth harmonic.

In Fig. 4, we show the dipole-emission properties of the harmonic H5 by calculating the time profiles and dynamical phases. The laser's parameters are the same as those in Fig. 2. The time profile is obtained by the wavelet transform of $d(t)$,

$$A_w(t_0,\omega) = \int d(t) w_{t_0,\omega}(t)\,\mathrm{d}t \equiv A_\omega(t), \tag{8}$$

here, $w_{t_0,\omega}(t) = \sqrt{\omega} W[\omega(t-t_0)]$. In our study, the Morlet wavelet is given by $W(x) = \frac{1}{\sqrt{\tau}} \mathrm{e}^{\mathrm{i}x} \mathrm{e}^{-\frac{x^2}{2\tau^2}}$. The dynamical phase $\theta(t)$ of the dipole-emission time profile $|A_\omega(t)|$ is obtained by $A_\omega(t) = |A_\omega(t)|\,\mathrm{e}^{-\mathrm{i}[\omega t + \theta(t)]}$. These instants can be construed as the electron–ion recollision times. For different laser wavelengths, we present the time profiles at harmonic energies of 10.59 eV, 10.54 eV, 10.51 eV, 10.46 eV, 10.44 eV, and 10.43 eV. Each of these specific energies corresponds to the harmonic peak labeled in the H5 inset of Fig. 2(a). From the time profiles presented in Figs. 4(a), 4(b), and 4(f), it can be observed that the H5 emission is mainly concentrated in the middle region of the laser field, spanning from the eighth to the 14th cycle, which corresponds to the transition 1 in Fig. 3. However, when the laser's wavelength is 532 nm, as depicted in Fig. 4(d), the H5 emission starts from the eighth cycle and continues until the end of the laser's field. During this period, the H5 radiation intensity is not only the strongest but also remains constant. This suggests that transitions 1 and 2 both contribute to the H5 emission. Figure 4 also reveals the dynamical phase of the fifth harmonic. It can be seen that the dynamical phase undergoes rapid oscillations as a function of recollision time, traversing the entire 0–2π domain, which would lead to both constructive and destructive interference in the dipole emission at different times. As shown in the shaded regions of Figs. 4(c) and 4(d), the dynamical phases are nearly uniform across the main emission periods. This uniformity results in constructive temporal interference of the bremsstrahlung radiation, indicating that the interference between transitions 1 and 2 plays a crucial role. In contrast, the dynamical phases change significantly in the other cases presented in Fig. 4. Despite the constructive interference observed in Fig. 4(c), the radiation at H5 is weaker than that at 532 nm. This is because the contributions from transitions 1 and 2 diminish throughout the entire emission process.

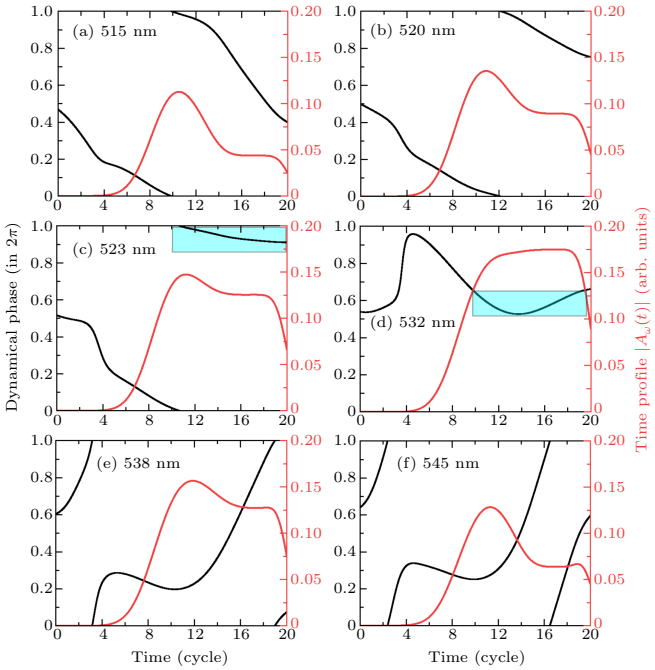


Fig. 4. The red solid lines indicate the time profiles of harmonic at energy (a) 10.59 eV, (b) 10.54 eV, (c) 10.51 eV, (d) 10.46 eV, (e) 10.44 eV, and (f) 10.43 eV with different laser wavelengths, which are corresponding to the harmonic peak in the H5 inset of Fig. 2(a). The black dots indicate the corresponding dynamical phases. The laser's intensity is 3.5×10^{14} W/cm^2 in all cases.

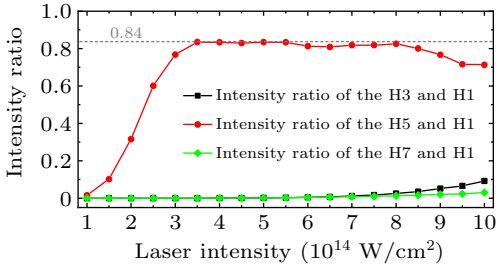


Fig. 5. The intensity ratios of the H3, H5, and H7 to the H1 respect to the laser intensities. The laser's wavelength is 532 nm.

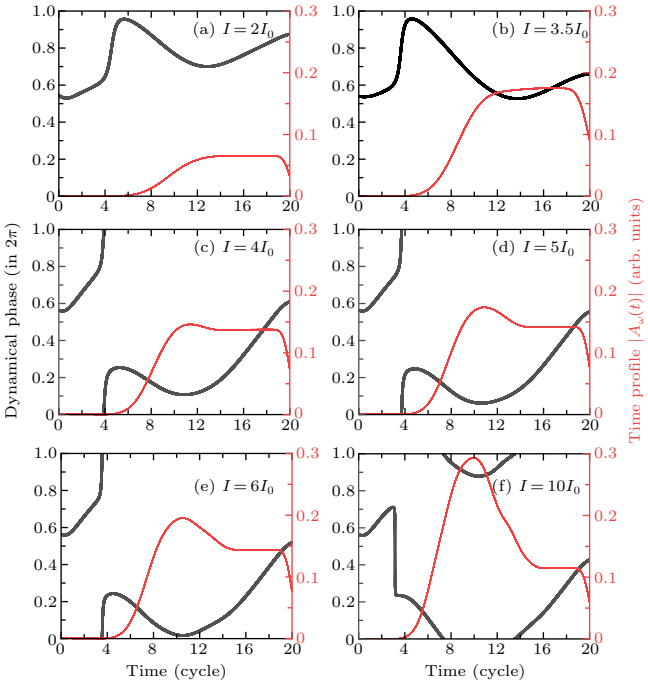


Fig. 6. The red solid lines indicate the time profiles at the peak of the fifth harmonic at laser intensity of (a) $2I_0$, (b) $3.5I_0$, (c) $4I_0$, (d) $5I_0$, (e) $6I_0$ and (f) $10I_0$. Here, $I_0 = 1.0 \times 10^{14}$ W/cm^2. The black dots indicate the corresponding dynamical phases. The laser's wavelength is 532 nm in all cases.

Among the three mechanisms that contribute to the enhanced H5, the AC Stark shift of the first excited $1\sigma_u$ state will directly affect the contribution of transition 2. Thus, it is essential to explore the correlation between laser intensity and the enhanced H5. Figure 5 presents the dependence of the harmonic peak ratios (H3/H1, H5/H1, and H7/H1) on the laser's intensity. The laser's wavelength is 532 nm in all cases. This shows clearly that, with increasing laser intensities from 1.0×10^{14} W/cm^2 to 1.0×10^{15} W/cm^2, the intensity ratios of the H3/H1 as well as H7/H1 remain very low, close to 0, and exhibit only minimal variation. In contrast, the H5/H1 displays a distinct behavior: it rises rapidly from 0 to 0.84 at intensities below approximately 3.5×10^{14} W/cm^2, beyond which it plateaus at a constant value of 0.84. At the laser intensity of 8.0×10^{14} W/cm^2, the H5/H1 begins decrease. To further investigate the physics behind this phenomenon, figure 6 presents the time profiles and the dynamical phases at the peak of the fifth harmonic with different laser intensities. One can see that, for the laser wavelength of 532 nm, when the laser intensity is 2.0×10^{14} W/cm^2 or 3.5×10^{14} W/cm^2, the H5 radiation starts from the eighth cycle and continues until the end of the laser field, which indicates that both transitions 1 and 2 occur. In addition, the dynamical phases are nearly uniform across the main emission periods. Thus, the interference between transitions 1 and 2 plays a crucial role. When the laser's intensity exceeds 3.5×10^{14} W/cm^2, as shown in Figs. 6(c)–6(f), not only does the amplitude of the time profiles from the 14th to the 19th cycle decrease, but the dynamical phases also change significantly. These factors reduce the contribution from both transition 2 and interference effect to the H5 radiation. Therefore, despite the significantly stronger radiation from transition 1 at laser intensity of 6×10^{14} W/cm^2 or 1×10^{15} W/cm^2, the intensity ratio of H5/H1 still begins to decline. That is to say, when the laser's intensity is 3.5×10^{14} W/cm^2, three distinct mechanisms all contribute to the H5 radiation, leading to high conversion efficiency. Meanwhile, the emission of other harmonics is virtually suppressed, which readily enables the generation of intense QM-XUV radiation.

Compared with symmetric atoms, the alignment of the molecule with respect to the polarization direction not only affects ionization of an electron but also affects harmonic emission.[33] Thus, in Fig. 7, we present the harmonic yields of the H3, H5, H7, H9, and H11 as a function of the orientation angle, the harmonic yield for the n-th order is obtained by integrating the spectrum from the $(n-0.5)$ to $(n+0.5)$ order. Because the transition between $1\sigma_u$ and $1\sigma_g$ states is not allowed at $\theta = 90°$ in a linear laser field, one can see that the H5 yield is comparable to that of the other order harmonics in the vicinity of 90°. However, the H5 yield is far higher than that of the other order harmonic at any other orientation angle. In particular, when the orientation angle is below 60°, it has no effect on the enhancement of the fifth harmonic. Although the yield of the fifth harmonic begins to decrease rapidly as the orientation angle increases from 60° to 90°, it remains significantly higher than that of other orders harmonic. For the other harmonic orders, the orientation angles have a great impact on the harmonic emission (see the inset of Fig. 7). This implies that in the experiment the alignment of H_2^+ does not play a crucial role in achieving a high conversion rate for the fifth harmonic.

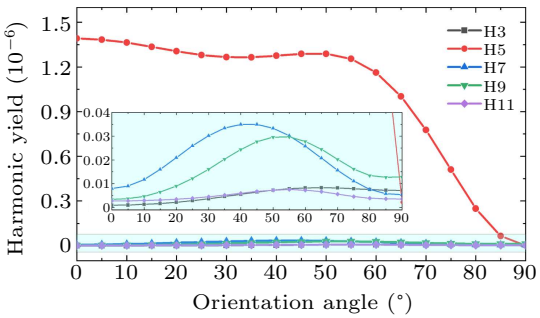


Fig. 7. The yield of the H3, H5, H7, H9, and H11 as a function of the orientation angles.

4. Conclusion

In conclusion, we have presented a detailed study of the high-efficiency harmonic radiation of H_2^+ in a linearly polarized laser field. By choosing an appropriate incident laser pulse, we observe the fifth harmonic with high conversion efficiency (with an H5/H1 intensity ratio of 0.84), while the ad-

jacent harmonics are dramatically suppressed. By varying the laser's wavelength, we compare the population of the $1\sigma_u$ state of H_2^+, time profiles and dynamical phases at the H5 peak intensity. The results reveal that the H5 enhancement arises from three distinct mechanisms: (1) transition 1: between the dressed states of the same excited state; (2) transition 2: a resonant transition between the Stark-shifted $1\sigma_u$ and $1\sigma_g$ states; and (3) interference effect: constructive interference between transitions 1 and 2. Furthermore, we find that the H5 conversion efficiency depends on the laser's intensity, reaching a maximum at 3.5×10^{14} W/cm^2 with a wavelength of 532 nm. Moreover, the alignment of H_2^+ is found to have only a minor influence on achieving a high conversion efficiency for the fifth harmonic. These findings are helpful for producing coherent QM-XUV sources in experiments.

Acknowledgments

Project supported by the National Natural Science Foundation of China (Grant No. 12264039) and the Natural Science Foundation of Ningxia (Grant No. 2024AAC03013).

References

[1] Bartels R A, Paul A, Green H, Kapteyn H C, Murnane M M, Backus S, Christov I P, Liu Y W, Attwood D and Jacobsen C 2002 *Science* **297** 376
[2] Klaiber M, Hatsagortsyan K Z, Müller C and Keitel C H 2008 *Opt. Lett.* **33** 411
[3] Winterfeldt C, Spielmann C and Gerber G 2008 *Rev. Mod. Phys.* **80** 117
[4] Ganeev R A 2007 *J. Phys. B* **40** R213
[5] Baker S, Robinson J S, Haworth C A, Teng H, Smith R A, Chirilă C C, Lein M, Tisch J W G and Marangos J P 2006 *Science* **312** 424
[6] Bian X B and Bandrauk A D 2012 *Phys. Rev. Lett.* **108** 263003
[7] Miller M R 2016 *Time Resolving Electron Dynamics in Atomic and Molecular Systems Using High-Harmonic Spectroscopy* Ph. D. thesis (University of Colorado Boulder)
[8] Zhai C Y, Wu Y M, Qin L L, Li X, Shi L, Zhang K, Kang S J, Li Z F, Li Y B, Tang Q B and Yu B H 2023 *Chin. Phys. B* **32** 073301
[9] Wang L, Xiao F, Song P, Tao W K, Sun X, Wang J C, Zheng Z G, Zhao J, Wang X W and Zhao Z X 2023 *Chin. Phys. Lett.* **40** 114203
[10] Song Y, Han S, Yang Y J and Guo F M 2024 *Chin. Phys. B* **33** 123201
[11] Corkum P B 1993 *Phys. Rev. Lett.* **71** 1994
[12] Ditmire T, Crane J K, Nguyen H, DaSilva L B and Perry M D 1995 *Phys. Rev. A* **51** R902(A)
[13] Kelkensberg F, Lefebvre C, Siu W, Ghafur O, Nguyen-Dang T T, Atabek O, Keller A, Serov V, Johnsson P, Swoboda M, Remetter T, LHuillier A, Zherebtsov S, Sansone G, Benedetti E, Ferrari F, Nisoli M, Lépine F, Kling M F and Vrakking M J 2009 *Phys. Rev. Lett.* **103** 123005
[14] Ravasio A, Gauthier D, Maia F R N C, Billon M, Caumes J P, Garzella D, Géléoc M, Gobert O, Hergott J F, Pena A M, Perez H, Carré B, Bourhis E, Gierak J, Madouri A, Mailly D, Schiedt B, Fajardo M, Gautier J, Zeitoun P, Bucksbaum P H, Hajdu J and Merdji H 2009 *Phys. Rev. Lett.* **103** 028104
[15] Sie E J, Rohwer T, Lee C and Gedik N 2019 *Nat. Commun.* **10** 3535
[16] Schmidt O, Bauer M, Wiemann C, Porath R, Scharte M, Andreyev O, Schönhense G and Aeschlimann M 2002 *Appl. Phys. B* **74** 223
[17] Nayak A, Orfanos I, Makos I, Dumergue M, Kühn S, Skantzakis E, Bodi B, Varju K, Kalpouzos C, Banks H I B, Emmanouilidou A, Charalambidis D and Tzallas P 2018 *Phys. Rev. A* **98** 023426
[18] Poletto L, Villoresi P, Benedetti E, Ferrari F, Stagira S, Sansone G and Nisoli M 2008 *J. Opt. Soc. Am. B* **25** B44
[19] Wei P F, Miao J, Zeng Z N, Li C, Ge X C, Li R X and Xu Z Z 2013 *Phys. Rev. Lett.* **110** 233903
[20] Wang X, Jin C and Lin C D 2014 *Phys. Rev. A* **90** 023416
[21] Rothhardt J, Hädrich S, Demmler S, Krebs M, Fritzsche S, Limpert J and Tünnermann A 2014 *Phys. Rev. Lett.* **112** 233002
[22] Ni J L, Yao J P, Zeng B, Chu W, Li G H, Zhang H S, Jing C R, Chin S L, Cheng Y and Xu Z 2011 *Phys. Rev. A* **84** 063846
[23] Kinder J F, Cipura F and Halfmann T 2021 *Phys. Rev. A* **103** 052808
[24] Heslar J, Telnov D A and Chu S I 2016 *Phys. Rev. A* **93** 063401
[25] Singh M, Fareed M A, Strelkov V, Grum-Grzhimailo A N, Magunov A, Laramée A, Légaré F and Ozaki T 2021 *Optica* **8** 1122
[26] Bengtsson S, Larsen E W, Kroon D, Camp S, Miranda M, Arnold C L, L'Huillier A, Schafer K J, Gaarde M B, Rippe L and Mauritsson J 2017 *Nat. Photonics* **11** 252
[27] Camp S, Schafer K J and Gaarde M B 2015 *Phys. Rev. A* **92** 013404
[28] Constant E, Garzella D, Breger P, Mével E, Dorrer C, Le Blanc C, Salin F and Agostini P 1999 *Phys. Rev. Lett.* **82** 1668
[29] Zhang B, Yuan J M and Zhao Z X 2012 *Phys. Rev. A* **85** 033421
[30] Tao L, McCurdy C W and Rescigno T N 2009 *Phys. Rev. A* **79** 012719
[31] Du L L, Wang Z B, Jin F C, Wang G L and Li P C 2023 *Laser Phys. Lett.* **20** 085302
[32] Zhou J W, Jiao Z H, Li P C and Zhou X X 2019 *Chin. Phys. B* **28** 103202
[33] Telnov D A and Chu S I 2007 *Phys. Rev. A* **76** 043412